Journal of Power Sources 196 (2011) 6085–6091

Contents lists available at ScienceDirect

Journal of Power Sources

journal homepage: www.elsevier.com/locate/jpowsour

Identical locations transmission electron microscopy study of Pt/C electrocatalyst degradation during oxygen reduction reaction

Francisco J. Perez-Alonso[a], Christian F. Elkjær[a], Signe S. Shim[a,b], Billie L. Abrams[a], Ifan E.L. Stephens[a], Ib Chorkendorff[a,*]

[a] Center for Individual Nanoparticle Functionality, Department of Physics, Building 312, Technical University of Denmark, DK-2800 Lyngby, Denmark
[b] IRD Fuel Cells A/S, Kullinggade 31, DK-5700 Svendborg, Denmark

ARTICLE INFO

Article history:
Received 14 December 2010
Received in revised form 22 January 2011
Accepted 27 March 2011
Available online 6 April 2011

Keywords:
Oxygen reduction
Identical locations transmission electron microscopy
Platinum
Corrosion
Fuel cell

ABSTRACT

The degradation mechanisms of Pt nanoparticles supported on Carbon have been characterized during oxygen reduction reaction (ORR) conditions using IL-TEM. A TEM grid is used as the sole working electrode allowing a direct correlation between the electrochemical response and the TEM analysis. We mainly observe a decrease in nanoparticle size with some particle disappearance and some particle sintering after potential cycling simulating the start-up and shut-down of a fuel cell. The observation of nanoparticles with reduced particle size provides evidence that dissolution phenomena are the main cause of degradation in Pt/C electrocatalysts, under ORR conditions.

© 2011 Elsevier B.V. All rights reserved.

1. Introduction

Proton exchange membrane fuel cells (PEMFC's) could play a major role in a future carbon-free society, with their ability to convert chemically stored energy into electricity. Arguably, the most significant obstacle preventing the widespread utilisation of PEMFC's is their prohibitively high cost. A significant portion of these costs can be traced to the poor activity and low stability of the Pt/C electrocatalysts at the cathode, which drives the oxygen reduction reaction (ORR) [1]. In recent years, significant improvements have been made to the activity of Pt by alloying it with other metals [2–5]. However, catalyst stability is also of critical importance for PEMFC applications [6–13].

This is an important issue for any new alloy catalyst. Even for the pure Pt there is a need to elucidate the mechanism for loosing activity during ORR. By understanding the fundamentals behind catalyst instability, we should ultimately be able to develop more fruitful strategies towards preventing Pt corrosion.

The instability of Pt is manifested as an effective loss of catalyst surface area. It is particularly pronounced when the cathode is exposed to high potentials, either during shut down/start up cycles or through inadvertent 'cell reversal'.

The loss of Pt surface area has been attributed to four different processes [7]:

(i) Ostwald ripening: the dissolution of metal ions from smaller particles, which diffuse and re-deposit onto larger particles.
(ii) Particle coalescence: the migration of Pt nanoparticles, leading to larger nanoparticles.
(iii) Dissolution of Pt nanoparticles and reprecipitation in the ionomer phase, forming new Pt nanoparticles which cannot contribute to the catalytic effect.
(iv) Detachment of nanoparticles from the carbon support.

Electrocatalyst degradation can be monitored, *in situ,* using electrochemical methods, albeit with little mechanistic insight. Transmission electron microscopy (TEM) is a powerful tool for examining the localised changes to catalyst structure during reaction conditions. However, most examples in the literature have relied on a *post-mortem* approach to TEM [14–17].

Recently, Mayrhofer et al. developed the identical location TEM (IL-TEM) technique [18–20]. Using this technique, they could observe *identical locations* of a sample examined *before* and *after* TEM analysis. In particular, their studies focussed on size distributions, the absolute number of nanoparticles and carbon support corrosion. Catalyst degradation was only observed when the sample was cycled to high potentials of 1.4 V, apparently caused by nanoparticle detachment [19,20]. On the contrary, electrocatalyst

* Corresponding author. Tel.: +45 4525 3170; fax: +45 4593 2399.
E-mail address: ibchork@fysik.dtu.dk (Ib Chorkendorff).

0378-7753/$ – see front matter © 2011 Elsevier B.V. All rights reserved.
doi:10.1016/j.jpowsour.2011.03.064

corrosion was not observed when the upper potential limit was confined to 1.05 V or 1.2 V.

In the current investigation, we use the IL-TEM technique to monitor Pt/C degradation under ORR conditions. We investigate Pt/C catalyst with a size of $\sim 2.3 \pm 0.4$ nm. In particular, we choose to investigate smaller nanoparticles as they are inherently less stable, meaning that their corrosion should be more easily observable than larger nanoparticles. This smaller size is also closer to the size given as the optimal size ($\sim$3 nm) for a maximum ORR mass activity [1].

We have modified Mayrhofer et al.'s original experiments [18–20], by using only a single working electrode, in the form of the TEM grid. In their experiments, the TEM grid was connected in parallel to another working electrode. Although Mayrhofer et al.'s configuration resulted in a more quantitative electrochemical response; our configuration allows a more direct comparison to be made between the electrochemical measurements and the TEM analysis.

Our experiments aim to simulate the effect of fuel cell load cycling (start up and shut down). This was achieved by cycling the TEM grid in O_2 saturated 0.1 M $HClO_4$, between 0.6 and 1.1 or 1.2 V at different scan rates.

2. Materials and methods

The Pt/C electrocatalyst was prepared using the inverse micelle method, with the aim of obtaining a narrow nanoparticle size distribution [21,22].

The H_2PtCl_6 precursor (0.005 M Pt concentration) was introduced into a solution containing a micro-heterogeneous environment of droplet-like inverse micelles formed by the surfactant didodecyldimethyl ammonium bromide (DDAB) (5 wt% DDAB content) in toluene. Then, an excess of $LiBH_4$ in tetrahydrofuran solution (final concentration of 0.08 M) is added to the micelle solution, whilst stirring, to achieve complete reduction of the metal particles.

Following this, a carbon black (Vulcan XC72R, CABOT)-DDAB-toluene suspension was prepared, with the appropriate weight of C to obtain a final metal content of 10 wt%. The mixture was sonicated for 30 min, resulting in a homogenous suspension. Then the nanoparticle solution was slowly added to the carbon black suspension. After 4 h of stirring, a destabilizing agent (ethanol 99.9%) was added dropwise to break the droplet-like inverse micelle equilibrium and precipitate the metal nanoparticles. This solution was continuously stirred to avoid particle agglomeration. The mixture was allowed to settle and decant overnight. The solid sample was recovered, further separated and washed with ethanol by centrifugation several times and dried at 60 °C overnight.

The electrochemical experiments were performed with Bio-Logic Instruments' VMP2 potentiostat, controlled by a computer. The rotating disc electrode (RDE) assemblies were provided by Pine Instruments Corporation. All glassware was cleaned in a 3:1 mixture of concentrated H_2SO_4:concentrated H_2O_2. This was subsequently sonicated and rinsed several times in Millipore water (>18.2 MΩ cm^{-1}, TOC < 5 ppb). A standard three-compartment glass cell was used for all electrocatalysis experiments. The electrolyte, 0.1 M $HClO_4$ (Aldrich, TraceSELECT® Ultra) was prepared using Millipore water (>18.2 MΩ cm^{-1}, TOC < 5 ppb). The counter electrode was a carbon cloth and the reference was Hg/Hg_2SO_4 electrode. However, all potentials were calibrated with respect to a reversible hydrogen electrode (RHE); the reference electrode was separated from the working electrode compartment using a ceramic frit. A TEM grid containing the Pt/C sample in contact with a glassy carbon electrode was used as the working electrode. All measurements were conducted at room temperature. Fig. 1 shows the configuration we have used whereby the TEM grid is placed inside a holder adapted for the rotating disk electrode measurements.

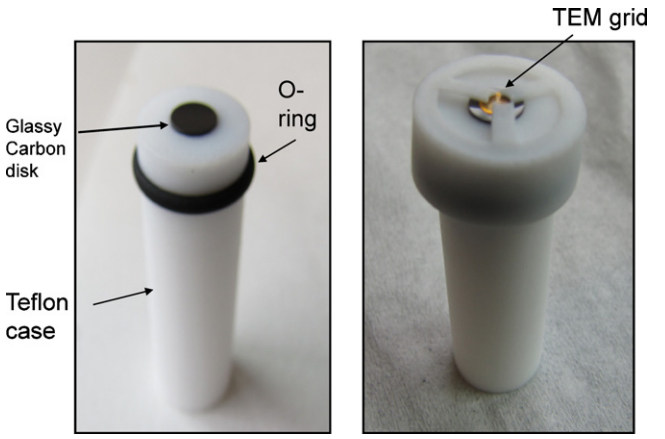

Fig. 1. Teflon holder adapted for the rotating disk electrode measurements using the Au TEM grid as working electrode.

For the corrosion tests, the working electrode was cycled between 0.6 and 1.1 V and between 0.6 and 1.2 V, without rotation, in O_2-saturated electrolyte. Two different scan rates were used, 50 and 200 mV s^{-1}. The effect of the total number of cycles was also studied by scanning the electrode between 0.6 and 1.1 V for 3000 or 30,000 cycles.

The ORR activity was carried out before and after the corrosion measurement, between 0 V and 1 V, at 20 mV s^{-1}, at 1600 RPM.

The TEM experiments were performed, using a TECNAI T20 electron microscope with a primary electron energy of 200 keV. For the TEM and electrochemical experiments, the Pt carbon supported catalyst was dispersed ultrasonically in isopropyl alcohol (Aldrich, 99.8%) to a concentration of 1.5 $mg_{catalyst}$ mL^{-1} for 30 min. A volume of 5 μL of the suspension was pippetted onto a gold-coated TEM grid with Lacey Carbon (300 mesh; Agar Scientific). We note that the catalyst loading on the grid was high in comparison to a conventional TEM experiment; this was in order to obtain a sufficiently high electrochemical response from the Pt/C on the TEM grid, when it was used as a working electrode. Despite the high catalyst loading, locations without overlapping catalyst particles were found on all the samples tested.

Prior to the ORR measurement, TEM was performed on several areas of the grid. The grid was then placed in the rotating disk set-up, the ORR was performed and the sample was then taken out again in order to repeat the TEM measurement. By using the appropriate coordinates, the same area on the TEM can be located.

3. Results and discussion

3.1. Validation of the concept

As a prerequisite, the Pt/C electrocatalyst on the TEM grid should not be affected by the transfer procedure from the microscope into the electrochemical cell and vice versa. The influence of the electrolyte was tested by submerging the TEM grid in 0.1 M $HCLO_4$ overnight. From the IL images, no changes in the state of the electrocatalyst were observed, proving the reliability of the method.

The intense radiation of the electron beam can also bring about unpredictable changes to the structure of the catalyst [23]. Such artefacts from the measurement are highly undesirable. In order to account for these changes, following the electrochemical measurements, TEM analysis was also performed at locations which had not previously been exposed to the electron beam, henceforth denoted as 'different locations' (DL). These results will be discussed

in detail in Sections 3.2 and 3.3. In brief, only slight differences were observed between locations which had not previously been exposed to the electron beam and the 'identical locations' (IL).

3.2. Accelerated corrosion tests between 0.6 and 1.2 V

Fig. 2 shows the TEM images, taken before and after the ORR measurement, taken in identical locations. The sample was subjected to 3000 cycles between 0.6 and 1.2 V at 200 mV s^{-1} in 0.1 M $HClO_4$. From Fig. 2, it was found that (i) the total number of particles have decreased, following the corrosion experiment, some examples of particle disappearance are marked with red circles in the images. This was also determined after a particle count for each TEM image. (ii) The particles have decreased in size, examples are marked with green circles in the images. These phenomena are also confirmed more quantitatively by the size distribution graphs in Fig. 3a. The reduction in size and disappearance of the nanoparticles (see Fig. 2) strongly suggest that Pt has dissolved under these conditions. Moreover, there may have been some reprecipitation and sintering according to the size distribution graphs in Fig. 3a.

It should be noted that there are slight differences between the nanoparticle size distributions obtained from the identical and the different locations. In principle, the trend observed in both cases is similar. However, in the images taken from different locations, there is a marginally higher frequency of larger nanoparticles, following the corrosion experiment. Since an appreciable number of particles had disappeared altogether, the number of nanoparticles counted from IL images to obtain the nanoparticle size distribution was much less than for DL images. Thus, considering that both distributions show the same trend, the small differences observed could in principle be due to statistical artefacts, rather than a real electron beam effect. A recent *in situ* TEM study by Simonsen et al. attempted to account for the possibility of electron beam induced degradation on supported Pt nanoparticles [23]. They only observed an increase in shrinkage of Pt nanoparticles when the electron beam was combined with an oxidising gas environment in the *in situ* TEM.

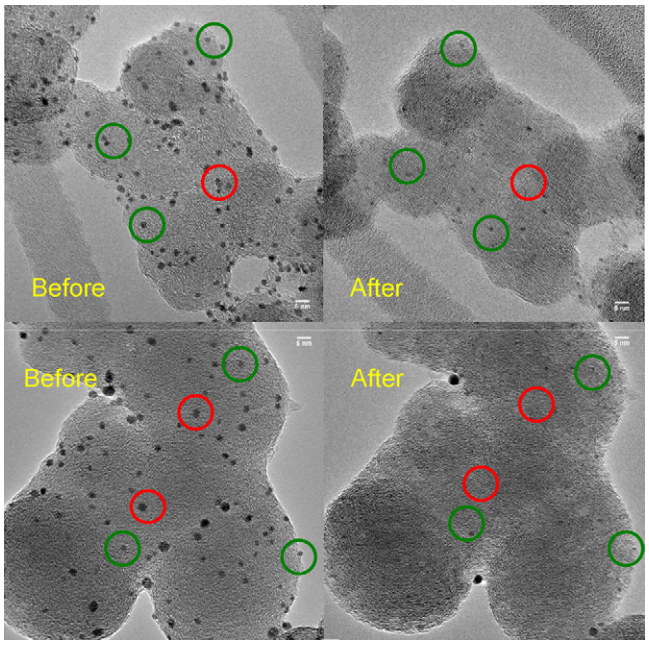

Fig. 2. IL-TEM images taken before and after accelerated corrosion test (sample was subjected to 3000 cycles between 0.6 and 1.2 V at 200 mV s^{-1} in 0.1 M $HClO_4$).

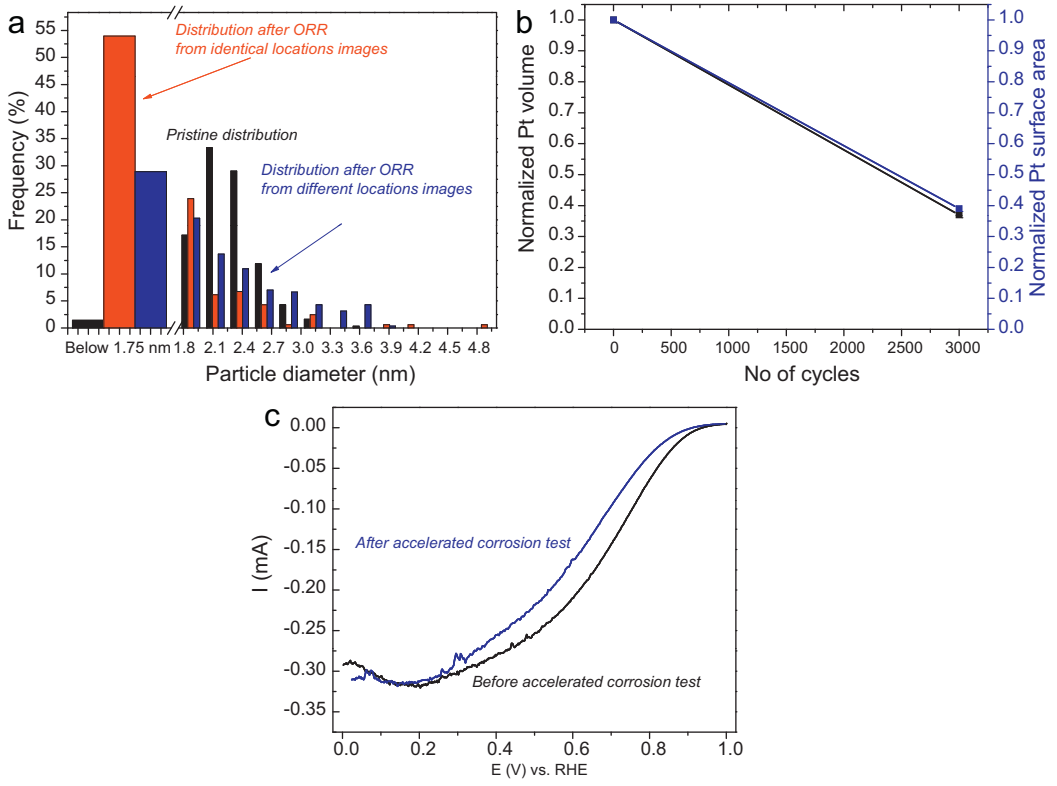

Fig. 3. (a) Nanoparticle size distribution graphs of sample subjected to 3000 cycles between 0.6 and 1.2 V, scan rate = 200 m V s^{-1} (black histogram: distribution from pristine sample (303 particles), red histograms: distribution after accelerated corrosion test from identical locations (156 particles), blue histograms (256 particles): distribution after accelerated corrosion test from different locations. (b) Normalized amount and surface area of Pt calculated before and after accelerated corrosion test from identical locations images. (c) ORR curve of sample before (black line) and after (blue line) accelerated corrosion test (For interpretation of the references to color in this figure legend, the reader is referred to the web version of the article.).

Since our TEM images were acquired in high vacuum, the electron beam effect is unlikely. Consequently, the slight differences observed between DL and IL distributions are ascribed to statistical artefacts.

Assuming a spherical shape for the nanoparticles, the area and the total volume of Pt present have been calculated from the IL images, before and after the ORR experiment, shown in Fig. 3b. A decrease of 60% in the volume and surface area of Pt was observed, as a result of the ORR corrosion experiment. Since a significant decrease in the Pt nanoparticle size was also observed, this loss of surface area is mainly attributed to the dissolution of Pt. This results correlates qualitatively with the electrochemical measurements of ORR activity, before and after the accelerated corrosion test, shown in Fig. 3c where a pronounced deactivation of 69 mV is observed in the half wave potential, $\Delta E_{1/2}$, after the accelerated corrosion test.

3.3. Accelerated corrosion tests between 0.6 and 1.1 V

Fig. 4 shows a different set of TEM images, where the catalyst has been cycled to the same conditions as in Fig. 2, albeit up to a maximum voltage of 1.1 V instead of 1.2 V, at 200 mV s^{-1}. On the basis of these images, there is some particle loss, movement and mild sintering, examples are noted with blue circles, but otherwise the particles have retained their shape during their exposure to ORR conditions. These observations are quantified in the size distribution graphs in Fig. 5a. The increased prevalence of larger particles, following the ORR, suggests that some sintering has occurred, most likely (albeit not definitively) through particle coalescence. The total volume of Pt calculated from identical locations remains unchanged while the Pt surface area decreases slightly (8%), again suggesting particle coalescence (see Fig. 5b). These results are consistent with the ORR activity measurements, where no deactivation was observed, as shown in Fig. 5c.

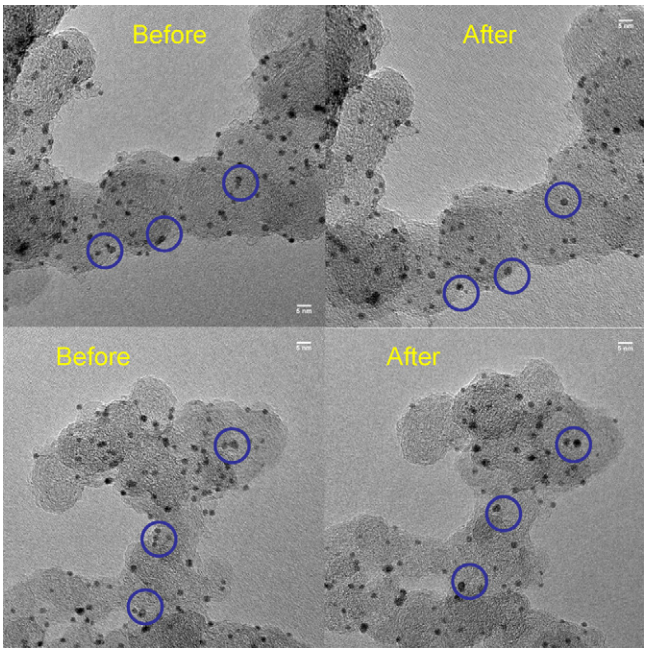

Fig. 4. IL-TEM images taken before and after accelerated corrosion test (sample was subjected to 3000 cycles between 0.6 and 1.1 V at 200 mV s^{-1} in 0.1 M $HClO_4$).

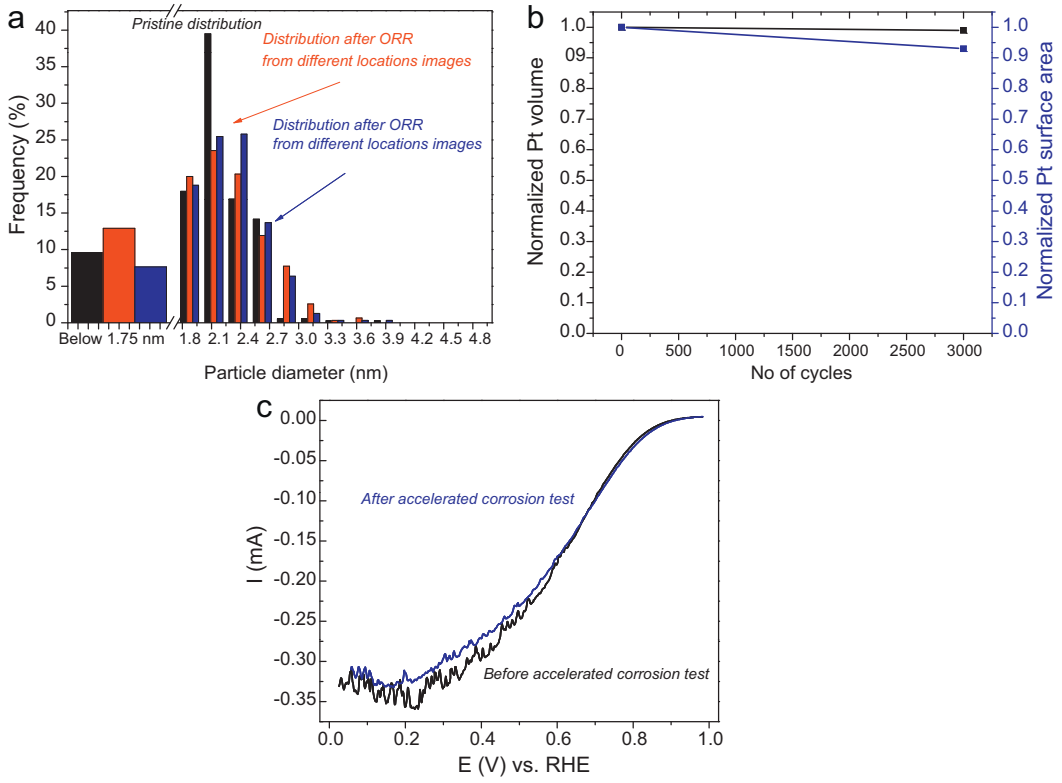

Fig. 5. (a) Nanoparticle size distribution graphs of sample subjected to 3000 cycles between 0.6 and 1.1 V, scan rate = 200 m V s^{-1} (black histogram: distribution from pristine sample (367 particles), red histograms: distribution after accelerated corrosion test from identical locations (311 particles), blue histograms: distribution after accelerated corrosion test from different locations (315 particles). (b) Normalized amount and surface area of Pt calculated before and after accelerated corrosion test from identical locations images. (c) ORR curve of sample before (black line) and after (blue line) accelerated corrosion test (For interpretation of the references to color in this figure legend, the reader is referred to the web version of the article.).

It is also worth noting that the particle distributions measured in the identical locations are roughly the same as those measured in different locations. This confirms that exposure to the electron beam does not have a significant effect on the experiments.

Since the effects on Pt degradation were not very significant after 3000 cycles of potential cycling between 0.6 and 1.1 V, the Pt/C catalyst was subjected to 30,000 cycles instead.

Fig. 6 displays the set of TEM images, before and after the accelerated corrosion test under these conditions. According to the images, there is some reduction in particle size (green circles), nanoparticle disappearance (red circles) and mild sintering (blue circles). In general, these effects are similar to those observed when the sample was cycled only 3000 times between 0.6 and 1.2 V. The size distribution graph, shown in Fig. 7a, confirms this trend: there are a higher number of large particles and there is an appreciable increase in the number of small nanoparticles, albeit to a lesser extent than the sample exposed to 3000 cycles up to 1.2 V. Notably, the catalyst exposed to 30,000 cycles does not seem to have sintered much more than the catalyst exposed to 3000 cycles. In summary, these results suggest that Pt dissolution is the main degradation mechanism under these conditions.

The total volume and the area of Pt present in the IL images have been calculated before and after the ORR experiment, as shown in Fig. 7b. In this case, a decrease of around 30% in Pt volume was observed after the ORR corrosion experiment. These results correspond qualitatively with the deactivation of 35 mV $\Delta E_{1/2}$ in ORR activity measured before and after aging, as shown in Fig. 7c. In this case, the loss in Pt surface area, at 22%, is less pronounced than the loss in its volume. This is in contrast to the experiment where the electrode was cycled for 3,000 cycles to 1.2 V (see Fig. 3b), where the proportion of surface area lost was equal to the proportion of volume lost. All of these results confirm that electrochemical dissolution of Pt is the major factor limiting this catalyst's durability with potential cycling for extended time periods.

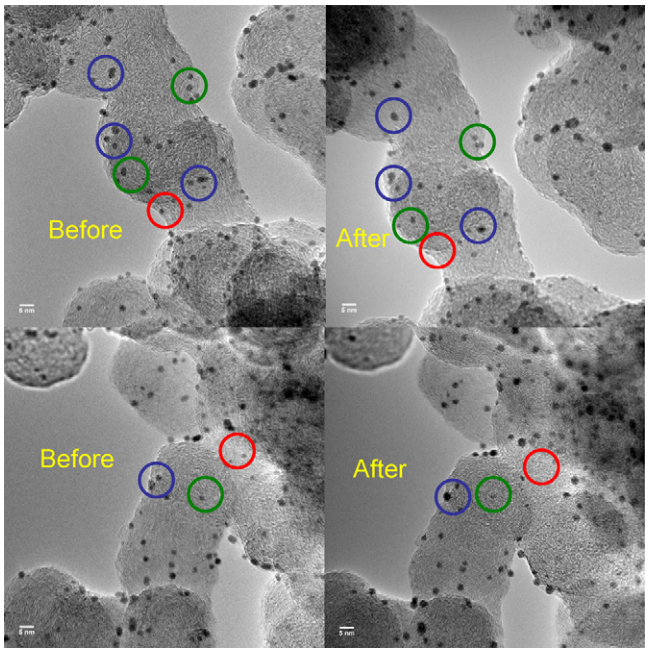

Fig. 6. IL-TEM images taken before and after accelerated corrosion test (sample was subjected to 30,000 cycles between 0.6 and 1.1 V at 200 mV s^{-1} in 0.1 M $HClO_4$).

However it is worthy to note that although our configuration allows a more direct comparison between the electrochemical

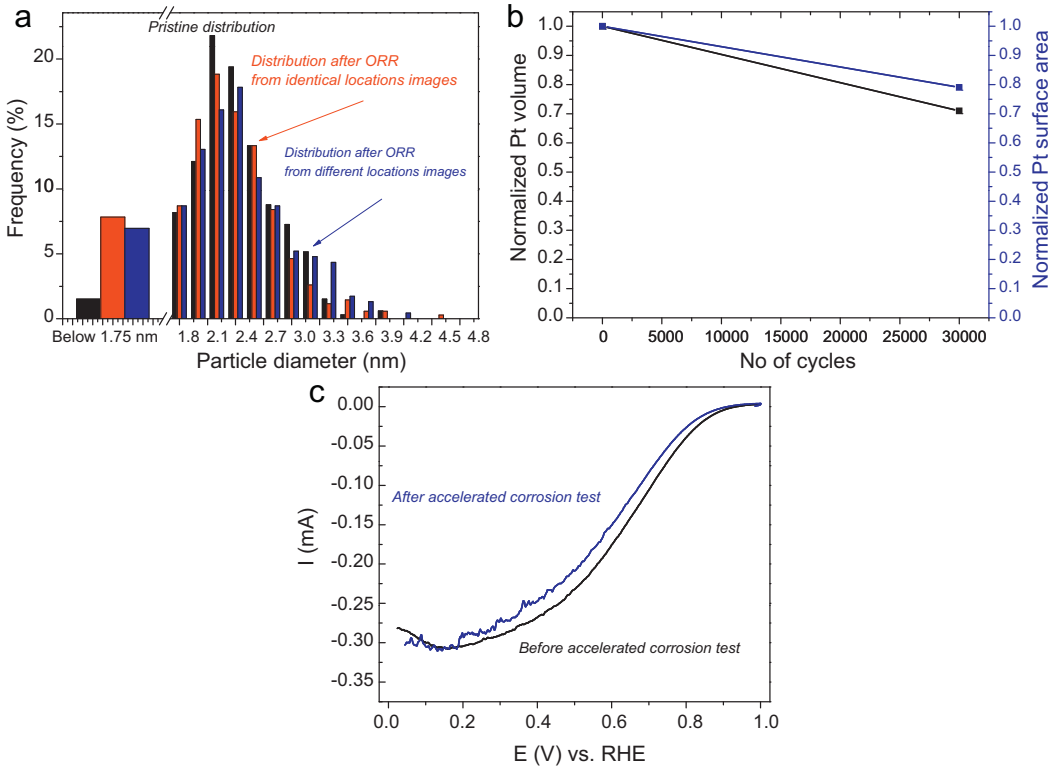

Fig. 7. (a) Nanoparticle size distribution graphs of sample subjected to 30,000 cycles between 0.6 and 1.1 V, scan rate = 200 m V s^{-1} (black histogram: distribution from pristine sample (303 particles), red histograms: distribution after accelerated corrosion test from identical locations (233 particles), blue histograms: distribution after accelerated corrosion test from different locations (230 particles). (b) Normalized amount and surface area of Pt calculated before and after accelerated corrosion test from identical locations images. (c) ORR curve of sample before (black line) and after (blue line) accelerated corrosion test (For interpretation of the references to color in this figure legend, the reader is referred to the web version of the article.).

measurements and the TEM analysis, the ORR curves obtained can be only interpreted qualitatively.

3.4. Effect of scan rate

In order to probe the effect of the scan rate on the phenomena observed, the experiments where the electrode was cycled 3000 times between 0.6 and 1.2 V and between 0.6 and 1.1 V were repeated a slower scan rate of 50 mV s^{-1}, instead of 200 mV s^{-1}. For both potential windows, the phenomena observed seemed to be independent of the scan rate (for brevity, these images have not been shown). This suggests that the Pt degradation is more dependent on the number of oxidation–reduction cycles, rather than the length of each cycle. Our observations are in agreement with the trends reported elsewhere in the literature [6].

3.5. Comparison to corrosion tests using 'thin film' rotating disk' electrode method

Although the use of a single working electrode in the form of a TEM grid allows a more direct comparison to be made between the electrochemical response and the TEM analysis, the electrochemical measurement is more qualitative than quantitative. Consequently, in the supplementary materials section, we present the results of equivalent measurements taken using the more conventional 'thin film' method [1,24]. Using the thin film method, a Pt/C ink is deposited onto the polished glassy carbon tip of a RDE (see the supplementary material). The loss of surface area was measured electrochemically by integrating the charge to adsorb H down to 0.05 V.

In brief, the thin film measurements showed that (a) the sample cycled up to 1.2 V for 3000 cycles showed a pronounced loss in surface area of ~50%, and a decrease in half wave potential of 25 mV (b) the sample cycled to 1.1 V for 3000 cycles showed a smaller loss in surface area and half wave potential, ~10% and ~8 mV, respectively, and (c) the sample cycled to 1.2 V for 30,000 cycles exhibited a more pronounced loss in the surface area and half wave potential, of 55% and of 35 mV, respectively. In (a) and (b) the electrochemically determined loss of surface area is comparable to that determined *ex situ* using the IL-TEM technique, whereas in (c) it seems to be more pronounced when the thin film method was used. The loss in half wave potentials is not exactly equivalent in the two methods. This is only to be expected, given the inherently more qualitative nature of the electrochemical measurement using the TEM grid as the sole working electrode.

Nonetheless, the generally good agreement between the two methods validates our approach for elucidating the mechanism of Pt/C degradation.

4. Discussion

According to the IL-TEM results, the degradation of our Pt/C electrocatalyst is primarily due to Pt dissolution, with some sintering, albeit to a lesser extent. To the best of our knowledge, the direct observation of Pt dissolution by the presence of particles with decreased size has not been reported previously.

The upper voltage limit value plays an important role during the accelerated corrosion test. Higher potentials (1.2 V versus 1.1 V) accelerate the dissolution of Pt. However, similar effects were observed when the sample was subjected to potential cycling between 0.6 and 1.1 V for longer time periods.

Our observations are also in good agreement with the main models described in the literature. Darling and Meyers [25,26] established a dissolution model for Pt particles, based on three different processes: electrochemical dissolution of the bare Pt surface, the oxidation of the Pt surface and the subsequent chemical dissolution of the oxidised Pt surface. They assumed that the chemical dissolution of oxidised Pt should be slow, and the electrochemical dissolution of Pt metal should predominate. Consequently, when the Pt surface is sufficiently oxidised, the underlying metal should be passivated against electrochemical dissolution. However, there has been some degree of debate as to whether Pt degradation in fuel cells occurs via the electrochemical dissolution of bare Pt or the chemical dissolution of oxidised Pt [7,25–29]. Kawahara et al. also suggest that the electrochemical reduction of PtO_2 could also play a role [30].

Regardless of the exact mechanism by which Pt dissolves, experimental evidence suggests that Pt dissolution should be enhanced considerably when the electrode is cycled to 1.2 V, instead of 1.1 V, in agreement with our own observations [25]. It is also known that Pt corrosion is enhanced when the voltage is cycled rather than under potentiostatic conditions [31].

It is worth perusing the differences between our own results and those of Mayrhofer et al., who using a similar IL-TEM methodology [20]. They observed very little, if any, degradation of their Pt/C catalyst when they cycled the electrode to 1.05 V or 1.2 V. However, we note that they used a different Pt/C catalyst, with a loading of ~50 wt% Pt, and particle diameter of 5 nm; in comparison, our catalyst had a loading of 10 wt% Pt and a smaller particle diameter of 2.5 nm.

There is a considerable body of theoretical and experimental evidence which would suggest that the stability of Pt nanoparticles is determined by their size [7,28,29,32,33]. Shao-Horn et al. made a thermodynamic estimation of particle size induced stability, using a thermodynamic analysis, based on the Gibbs Thomson equation and an extension of the Darling model [7]. They predicted an exponential increase in dissolution rate, as the particle size is decreased below 5 nm. Thus, the model established a critical change in lifetimes of nanoparticle to dissolve completely on the scale of many thousands of hours for 5 nm nanoparticles to the scale of ten to hundreds of hours for 2 nm ones.

Shao-Horn's analysis is also supported by the recent investigations of Tang et al. [28,29]. They directly measured the dissolution potential of individual Au supported Pt nanoparticles, using electrochemical scanning tunnelling microscopy (EC-STM). They supported their data with a series of density functional theory (DFT) calculations. Their theoretical model extended the simple Gibbs Thomson analysis, accounting for the role of surface passivation and site specific dissolution as a function of particle size. Both experiment and theory showed that the dissolution potential had an almost linear increase with particle size. For particles below 4 nm in diameter, the electrochemical dissolution of metallic Pt should be thermodynamically favoured. However, for nanoparticles above 4 nm in diameter, hydroxyl adsorption should occur at lower potentials than electrochemical Pt metal dissolution; in this case if dissolution occurs, it would be via the chemical dissolution of oxidised Pt.

On the basis of the aforementioned studies, it is perhaps unsurprising that our Pt nanoparticles, at 2.3 nm, should be more susceptible to dissolution than those of Mayrhofer et al., with a diameter of 5 nm.

In summary, in this work we report a reduction in nanoparticle size, for carbon supported Pt catalysts. The experimental conditions were chosen to simulate the start up and shut down cycles of a fuel cell. Our observations provide direct, microscopic evidence that dissolution phenomena are the main cause of degradation in Pt/C electrocatalysts, under ORR conditions.

The kinetics of Pt dissolution is dependent upon nanoparticle size, shape and their interaction with the support. An optimisation of these parameters would greatly reduce Pt surface area loss during voltage cycling. The extent of Pt dissolution seems to

be governed by a complex interplay between the electrochemical dissolution of Pt, the anodic formation of oxidised Pt and its subsequent dissolution. Further investigations are needed to develop a deeper understanding of Pt dissolution. With greater mechanistic insight, new strategies could be developed to avoid or restrict Pt corrosion during fuel cell operation.

5. Conclusions

This study has demonstrated the use of the IL-TEM method with the TEM grid as the sole working electrode. This configuration allowed a qualitative, albeit direct correlation to be made between the electrochemical response and the TEM analysis.

The Pt/C electrocatalyst was subjected to potential cycling, simulating the start-up and shut-down of a fuel cell. A reduction in particle size, with some particle disappearance, proved that Pt dissolution is the dominant mechanism of degradation. Some sintering occurred in all of experiments developed, most likely (albeit not definitively) through particle coalescence.

Increasing the upper voltage limit value (1.2 V) accelerated the corrosion of Pt. However, the same effects were also observed when the sample was subjected to potential cycling until 1.1 V for longer time periods.

Acknowledgements

We gratefully acknowledge funding from the Danish Strategic Research Council's HyCycle program, the Danish Council for Technology and Innovation's FTP program. IELS acknowledges funding from PSO-financed ForskEL/EL grant (High Performance MEA's, project 010076) from energinet.dk. FJPA acknowledges funding from the Spanish Government Ministry of Education's, "Programa Nacional de Movilidad de Recursos Humanos del Plan Nacional de I-D+I 2008–2011". The Center for Individual Nanoparticle Functionality is supported by the Danish National Research Foundation.

Appendix A. Supplementary data

Supplementary data associated with this article can be found, in the online version, at doi:10.1016/j.jpowsour.2011.03.064.

References

[1] H.A. Gasteiger, S.S. Kocha, B. Sompalli, F.T. Wagner, Applied Catalysis B-Environmental 56 (2005) 9–35.
[2] P. Strasser, S. Koh, T. Anniyev, J. Greeley, K. More, C.F. Yu, Z.C. Liu, S. Kaya, D. Nordlund, H. Ogasawara, M.F. Toney, A. Nilsson, Nature Chemistry 2 (2010) 454–460.
[3] V. Stamenkovic, B.S. Mun, K.J.J. Mayrhofer, P.N. Ross, N.M. Markovic, J. Rossmeisl, J. Greeley, J.K. Norskov, Angewandte Chemie-International Edition 45 (2006) 2897–2901.
[4] V.R. Stamenkovic, B.S. Mun, M. Arenz, K.J.J. Mayrhofer, C.A. Lucas, G.F. Wang, P.N. Ross, N.M. Markovic, Nature Materials 6 (2007) 241–247.
[5] J. Greeley, I.E.L. Stephens, A.S. Bondarenko, T.P. Johansson, H.A. Hansen, T.F. Jaramillo, J. Rossmeisl, I. Chorkendorff, J.K. Norskov, Nature Chemistry 1 (2009) 552–556.
[6] R. Borup, J. Meyers, B. Pivovar, Y.S. Kim, R. Mukundan, N. Garland, D. Myers, M. Wilson, F. Garzon, D. Wood, P. Zelenay, K. More, K. Stroh, T. Zawodzinski, J. Boncella, J.E. McGrath, M. Inaba, K. Miyatake, M. Hori, K. Ota, Z. Ogumi, S. Miyata, A. Nishikata, Z. Siroma, Y. Uchimoto, K. Yasuda, K.I. Kimijima, N. Iwashita, Chemical Reviews 107 (2007) 3904–3951.
[7] Y. Shao-Horn, W.C. Sheng, S. Chen, P.J. Ferreira, E.F. Holby, D. Morgan, Topics in Catalysis 46 (2007) 285–305.
[8] J. Zhang, K. Sasaki, E. Sutter, R.R. Adzic, Science 315 (2007) 220–222.
[9] S. Zhang, X.-Z. Yuan, J.N.C. Hin, H. Wang, K.A. Friedrich, M. Schulze, Journal of Power Sources 194 (2009) 588–600.
[10] Y.Y. Shao, G.P. Yin, Y.Z. Gao, Journal of Power Sources 171 (2007) 558–566.
[11] S. Chen, H.A. Gasteiger, K. Hayakawa, T. Tada, Y. Shao-Horn, Journal of the Electrochemical Society 157 (2010) A82–A97.
[12] F. Maillard, L. Dubau, J. Durst, M. Chatenet, J. Andre, E. Rossinot, Electrochemistry Communications 12 (2010) 1161–1164.
[13] E. Guilminot, A. Corcella, M. Chatenet, F. Maillard, F. Charlot, G. Berthome, C. Iojoiu, J.Y. Sanchez, E. Rossinot, E. Claude, Journal of the Electrochemical Society 154 (2007) B1106–B1114.
[14] P.J. Ferreira, G.J. la O, Y. Shao-Horn, D. Morgan, R. Makharia, S. Kocha, H.A. Gasteiger, Journal of the Electrochemical Society 152 (2005) A2256–A2271.
[15] K. Yasuda, A. Taniguchi, T. Akita, T. Ioroi, Z. Siroma, Physical Chemistry Chemical Physics 8 (2006) 746–752.
[16] T. Akita, A. Taniguchi, J. Maekawa, Z. Sirorna, K. Tanaka, M. Kohyama, K. Yasuda, Journal of Power Sources 159 (2006) 461–467.
[17] P. Yu, M. Pemberton, P. Plasse, Journal of Power Sources 144 (2005) 11–20.
[18] K.J.J. Mayrhofer, M. Hanzlik, M. Arenz, Electrochimica Acta 54 (2009) 5018–5022.
[19] K.J.J. Mayrhofer, J.C. Meier, S.J. Ashton, G.K.H. Wiberg, F. Kraus, M. Hanzlik, M. Arenz, Electrochemistry Communications 10 (2008) 1144–1147.
[20] K.J.J. Mayrhofer, S.J. Ashton, J.C. Meier, G.K.H. Wiberg, M. Hanzlik, M. Arenz, Journal of Power Sources 185 (2008) 734–739.
[21] J.P. Wilcoxon, B.L. Abrams, Chemical Society Reviews 35 (2006) 1162–1194.
[22] P. Hernandez-Fernandez, S. Rojas, P. Ocon, J.L.G. de la Fuente, P. Terreros, M.A. Pena, J.L. Garcia-Fierro, Applied Catalysis B-Environmental 77 (2007) 19–28.
[23] S.B. Simonsen, I. Chorkendorff, S. Dahl, M. Skoglundh, J. Sehested, S. Helveg, Journal of the American Chemical Society 132 (2010) 7968–7975.
[24] K.J.J. Mayrhofer, D. Strmcnik, B.B. Blizanac, V. Stamenkovic, M. Arenz, N.M. Markovic, Electrochimica Acta 53 (2008) 3181–3188.
[25] R.M. Darling, J.P. Meyers, Journal of the Electrochemical Society 150 (2003) A1523–A1527.
[26] R.M. Darling, J.P. Meyers, Journal of the Electrochemical Society 152 (2005) A242–A247.
[27] S.G. Rinaldo, J. Stumper, M. Eikerling, Journal of Physical Chemistry C 114 (2010) 5773–5785.
[28] L. Tang, B. Han, K. Persson, C. Friesen, T. He, K. Sieradzki, G. Ceder, Journal of the American Chemical Society 132 (2009) 596–600.
[29] L. Tang, X. Li, R.C. Cammarata, C. Friesen, K. Sieradzki, Journal of the American Chemical Society 132 (2010) 11722–11726.
[30] S. Kawahara, S. Mitsushima, K. Ota, N. Kamiya, ECS Transactions 3 (2006) 625–631.
[31] K. Kinoshit, Jt Lundquis, P. Stonehar, Journal of Electroanalytical Chemistry 48 (1973) 157–166.
[32] R. Makharia, S. Kocha, P. Yu, M.A. Sweikart, W. Gu, F. Wagner, H.A. Gasteiger, ECS Transactions 1 (2006) 3–18.
[33] R. Jinnouchi, E. Toyoda, T. Hatanaka, Y. Morimoto, The Journal of Physical Chemistry C 114 (2010) 17557–17568.